Electronic Supplementary Material (ESI) for Journal of Materials Chemistry A.


**Electronic Supplementary Information**

# Nickel-Rich Layered $LiNi_{1-x}M_xO_2$ ($M$ = Mn, Fe, and Co) Electrocatalysts with High Oxygen Evolution Reaction Activity

Veronica Augustyn, Soosairaj Therese, Travis C. Turner, and Arumugam Manthiram

Materials Science and Engineering Program & Texas Materials Institute
The University of Texas at Austin
Austin, TX 78712, USA

**Table S1**. BET surface areas of selected $LiNi_{1-x}M_xO_2$ ($M$ = Mn, Fe, and Co) compounds investigated for the OER

| Composition | BET Surface Area ($m^2\ g^{-1}$) |
|---|---|
| $LiNiO_2$, 850°C | 1.2 |
| $LiNi_{0.9}Co_{0.1}O_2$, 850°C | 1.3 |
| $LiNi_{0.9}Mn_{0.1}O_2$, 850°C | 1.2 |
| LNFO, 750°C | 3.2 |

**Figure S1**. 7-point BET data for $LiNiO_2$, $LiNi_{0.9}Co_{0.1}O_2$, $LiNi_{0.9}Mn_{0.1}O_2$, and LNFO used to calculate the surface areas shown in Table S1.

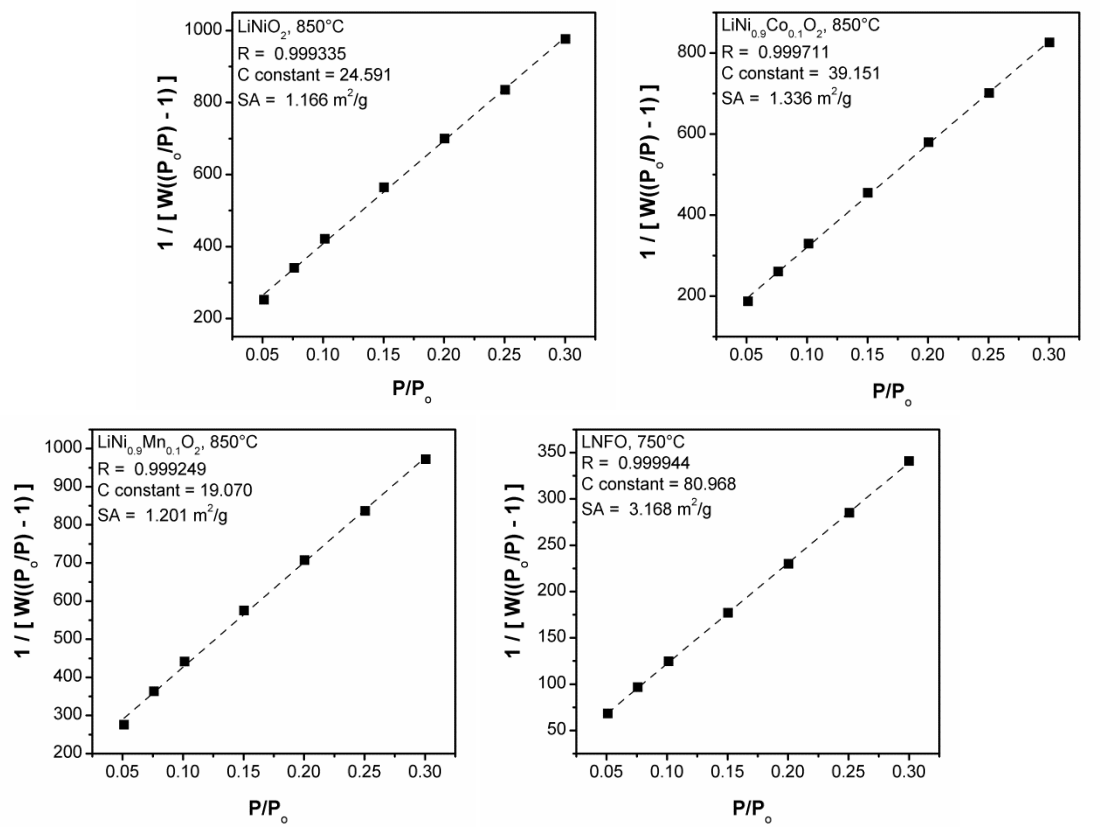

**Table S2**. Capacity (Q) of pre-OER redox peaks calculated from third cycle CVs at 10 mV $s^{-1}$ for $LiNi_{1-x}M_xO_2$ and $Ni_{1-x}M_x(OH)_x$

| Composition | $Q_{anodic}$ (C $g^{-1}$) | $Q_{cathodic}$ (C $g^{-1}$) |
|---|---|---|
| LNO | 2.7 | 5.0 |
| $Ni(OH)_2$ | 146.6 | 169.9 |
| LNFO | 1.2 | 3.9 |
| $Ni_{0.9}Fe_{0.1}(OH)_x$ | 38.7 | 40.4 |
| LNMO | 10.7 | 21.6 |
| $Ni_{0.7}Mn_{0.3}(OH)_x$ | 17.5 | 17.7 |
| LNMFO | 1.4 | 3.8 |
| $Ni_{0.7}Mn_{0.2}Fe_{0.1}(OH)_x$ | 12.3 | 18.5 |
| LNCO | 5.2 | 6.8 |
| $Ni_{0.7}Co_{0.3}(OH)_x$ | 37.3 | 38.1 |
| LNCFO | 18.2 | 29.0 |
| LNCFO-$\delta$ | 32.0 | 43.8 |
| $Ni_{0.7}Co_{0.3}Fe_{0.1}(OH)_x$ | 26.9 | 33.2 |

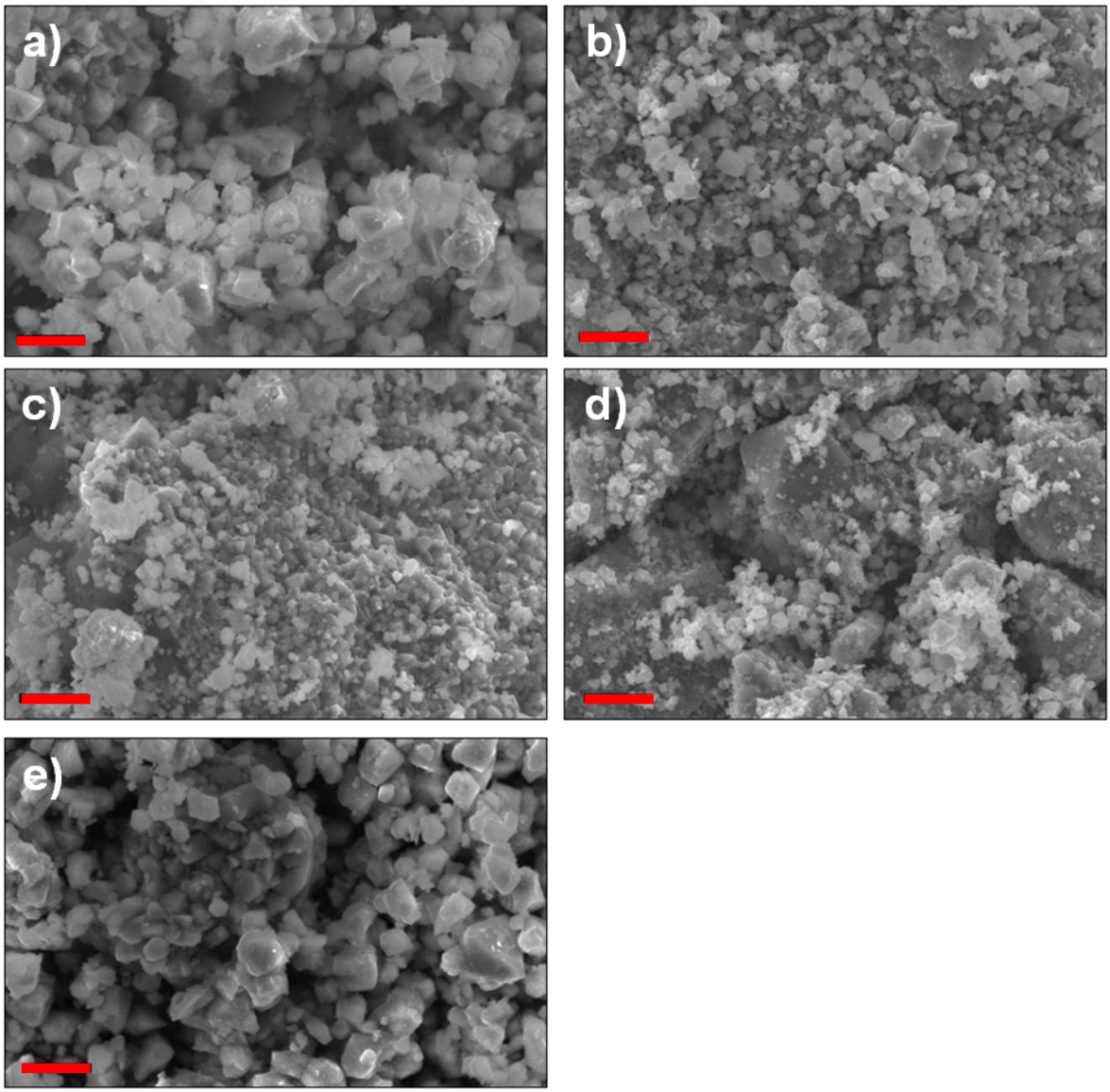


**Figure S2**. SEM images of the $LiNi_{1-x}M_xO_2$ samples, synthesized at 850 °C in air, investigated for the OER: (a) $LiNiO_2$, (b) $LiNi_{0.95}Mn_{0.05}O_2$, (c) $LiNi_{0.9}Mn_{0.1}O_2$, (d) $LiNi_{0.85}Mn_{0.15}O_2$, and (e) $LiNi_{0.9}Co_{0.1}O_2$. Scale bar = 5 µm.

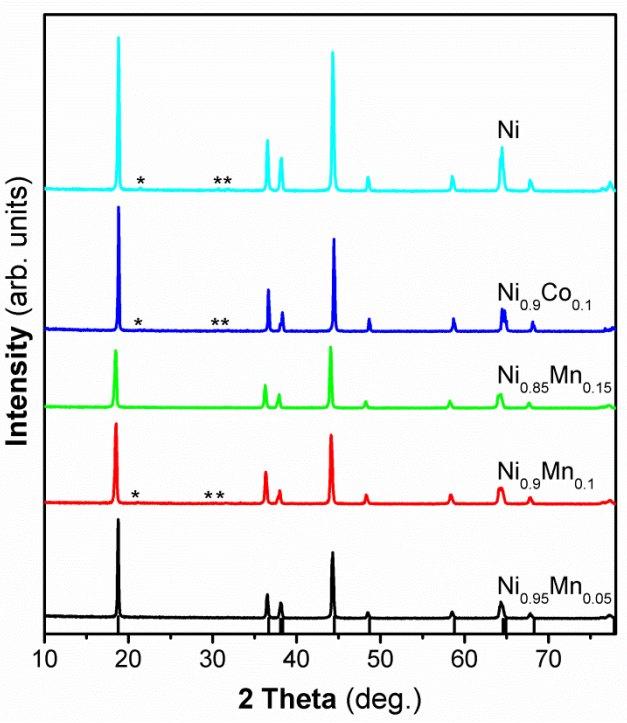


**Figure S3**. XRD patterns of $LiNi_{1-x}M_xO_2$ synthesized at 850°C in air. The samples all crystallize in the O3 layered structure; the reference pattern is shown at the bottom (PDF# 00-056-1441, $LiNi_{0.85}Co_{0.15}O_2$). * denotes $Li_2CO_3$ impurity present due to the high-temperature synthesis in air.

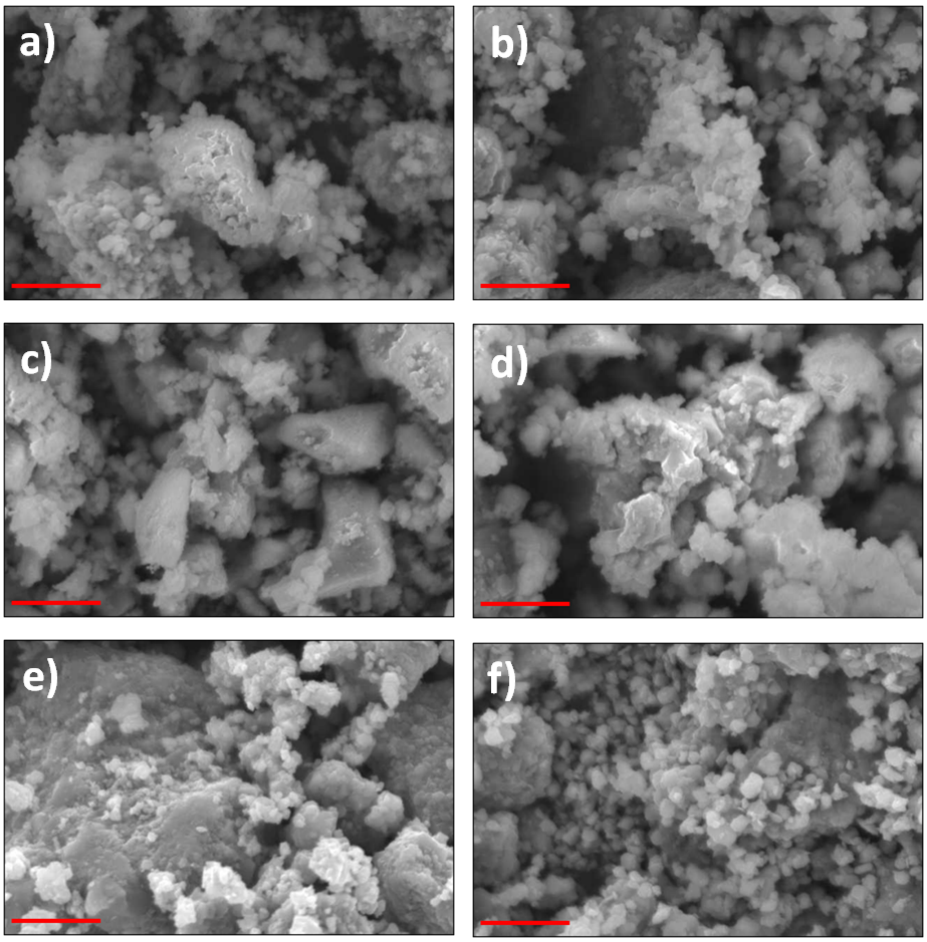


**Figure S4**. SEM images of the $LiNi_{1-x}M_xO_2$ samples, synthesized at 750°C in $O_2$, investigated for the OER: (a) LNO, (b) LNFO, (c) LNMO, (d) LNMFO, (e) LNCO, (f) LNCFO-$\delta$. Scale bar = 5 μm.

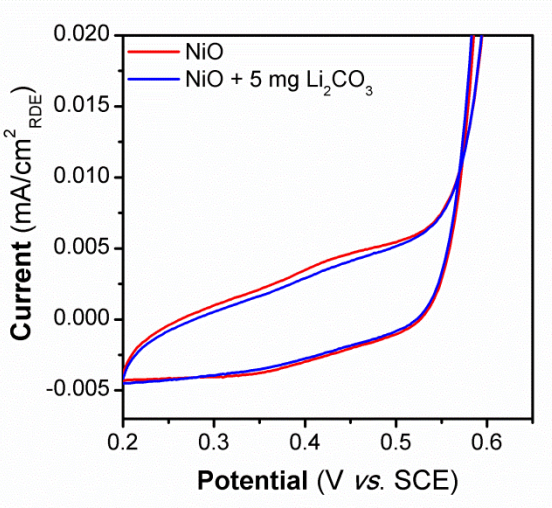


**Figure S5**. As Ni content and Li content increase during high-temperature synthesis, Ni-rich Li*M*$O_2$ tend to form $Li_2CO_3$ impurity even in an oxygen-rich atmosphere. To explore the effect of the small amount of $Li_2CO_3$ impurity present in the samples on OER activity, 5 mg of $Li_2CO_3$ was added to the standard ink preparation of NiO (25 mg active material, 5 mg acetylene black, 154 µL of Nafion/0.1 M NaOH solution, 4.5 mL water, and 0.5 mL isopropanol). There was no observed effect of $Li_2CO_3$ on the pre-OER redox peaks or the OER onset potential. We hypothesize that the efficient rotation of the RDE (1600 rpm) quickly diffuses away the carbonate impurity into the electrolyte (~ 150 mL of 0.1 M KOH).

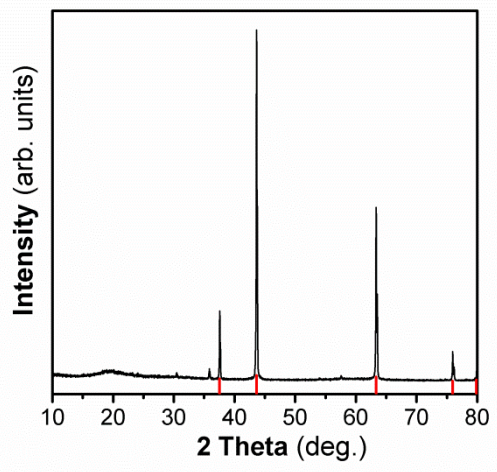


**Figure S6**. XRD pattern of $LiFeO_2$ (ICP composition: $Li_{1.01}Fe_{0.99}O_2$) synthesized by a solid-state reaction between $Fe_2O_3$ and $Li_2CO_3$ at 750 °C in air. The major reflections correlate with the disordered cubic structure of $\alpha$-$LiFeO_2$ (PDF# #00-017-0938).

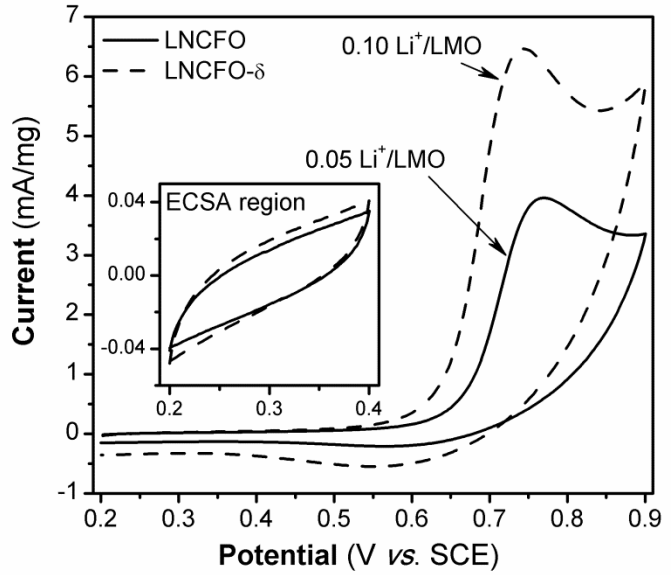


**Figure S7**. First cycle CVs in 0.5 M $Li_2SO_4$ at 10 mV $s^{-1}$ for LNCFO and LNCFO-$\delta$. The capacity associated with the anodic peak current corresponds to the irreversible extraction of $Li^+$ from Li$M$O$_2$. More $Li^+$ is extracted from LNCFO-$\delta$ (which also contained more $Li^+$ in the as-synthesized state) and this compound had higher OER activity.

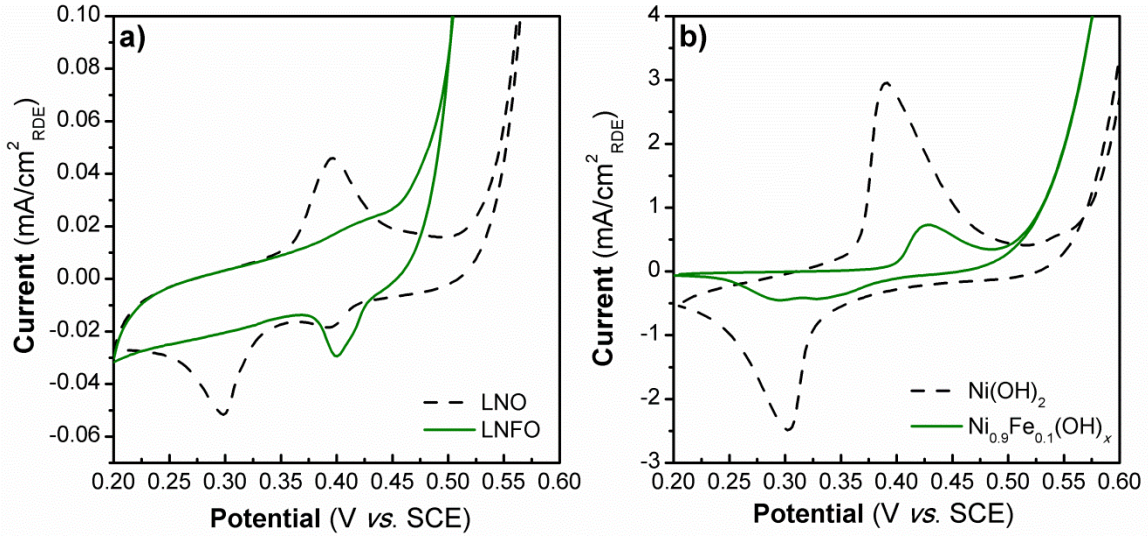


**Figure S8**. Comparison of the pre-OER redox peaks in (a) LNO and LNFO (synthesized at 750 °C in flowing $O_2$) and (b) $Ni(OH)_2$ and $Ni_{0.9}Fe_{0.1}(OH)_x$ synthesized at room temperature and used as precursors for the solid-state synthesis.

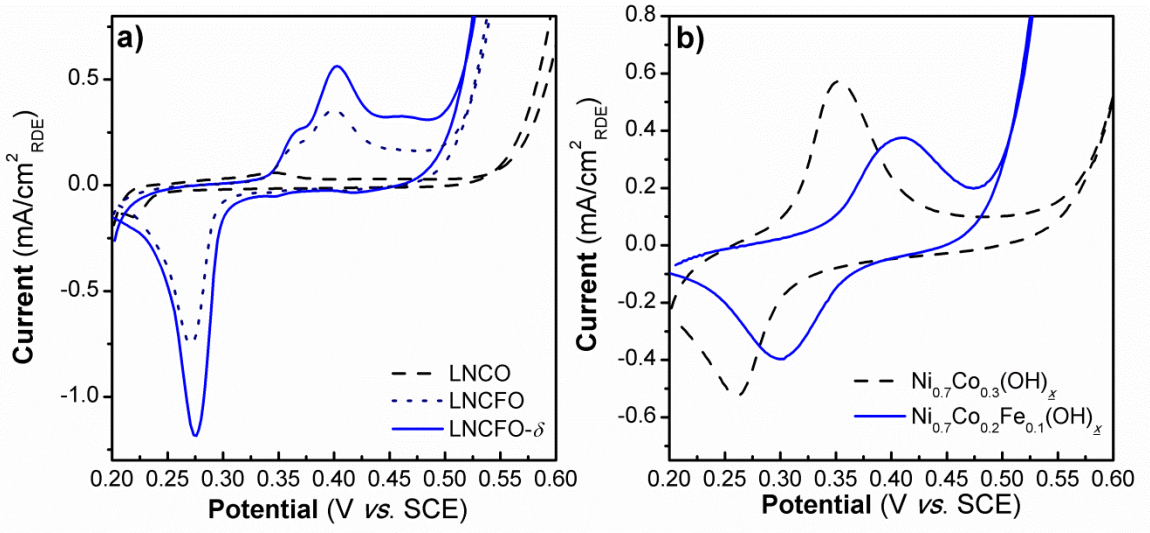


**Figure S9**. Comparison of the pre-OER redox peaks in (a) LNCO, LNCFO, and LNCFO-$\delta$ (synthesized at 750 °C in flowing $O_2$) and (b) $Ni_{0.7}Co_{0.3}(OH)_x$ and $Ni_{0.7}Co_{0.2}Fe_{0.1}(OH)_x$ synthesized at room temperature and used as precursors for the solid-state synthesis.

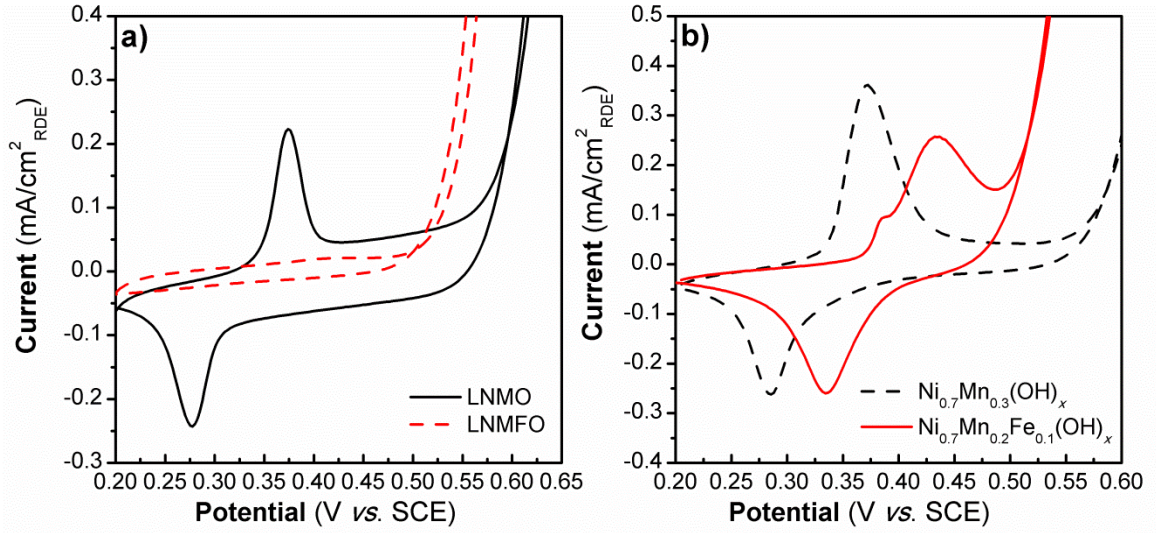


**Figure S10**. Comparison of the pre-OER redox peaks in (a) LNMO and LNMFO (synthesized at 750 °C in flowing $O_2$) and (b) $Ni_{0.7}Mn_{0.3}(OH)_x$ and $Ni_{0.7}Mn_{0.2}Fe_{0.1}(OH)_x$ synthesized at room temperature and used as precursors for the solid-state synthesis.

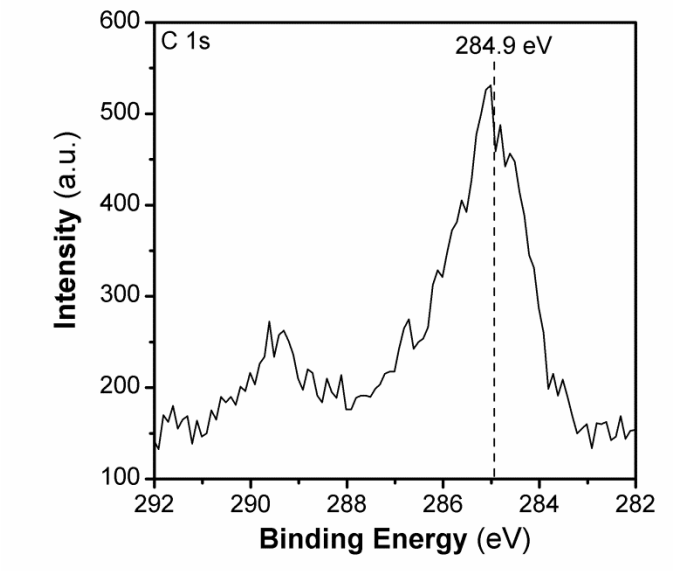


**Figure S11**. XPS of the C 1s spectrum of LNFO. The tallest peak, corresponding to adsorbed adventitious hydrocarbons (284.9 eV), was used for calibration of the spectrum.